Polymerization of cellulose nanocrystals-based Pickering HIPE towards green porous materials

H. Dupont, C. Fouché, M.-A. Dourges, V. Schmitt, V. Héroguez

Polymerization of cellulose nanocrystals-based Pickering HIPE towards green porous materials

H. Dupont[1,2], C. Fouché[1,2], M.-A. Dourges[3], V. Schmitt[1 *], V. Héroguez[2 *]

[1] Centre de Recherche Paul Pascal, UMR 5031 Univ. Bordeaux CNRS, 115 avenue du Dr Albert Schweitzer, 33600 Pessac, France.

[2] Laboratoire de Chimie des Polymères Organiques, Univ. Bordeaux, CNRS, Bordeaux INP, UMR 5629, Bordeaux, 16 Avenue Pey-Berland, F-33607 Pessac, France.

[3] Institut des Sciences Moléculaires, Université de Bordeaux, UMR 5255 CNRS, 351 Cours de la Libération, 33405 Talence, France.

*** corresponding authors**
veronique.schmitt@crpp.cnrs.fr
heroguez@enscbp.fr

Abstract

Porous materials were produced based on high internal phase emulsions (HIPE) formulation stabilized by modified cellulose nanocrystals (CNCs). CNCs were first modified with bromoisobutyryl bromide and used as Pickering emulsion stabilizers to formulate highly concentrated inverse emulsions. Solid foams with an open porosity were successively produced by free radical polymerization of styrene/divinylbenzene continuous phase. The final materials were characterized regarding their cell size distribution, porosity and mechanical properties and then compared with well-known styrene/DVB polyHIPE stabilized either with usual surfactants or solid particles.

Keywords: cellulose nanocrystals; Pickering; High Internal Phase Emulsions (HIPE); Polymerized HIPE (PolyHIPE)

1. Introduction

Highly porous**,** open-celled, low density polymer foams are very attractive materials for a wide range of applications in many fields (Bhumgara, 1995; Gibson and Ashby, 2014; Yang et al., 2017), catalysis, tissue engineering, acoustics, thermal insulator, filtration. Emulsion templating emerged as a way to easily obtain such porous materials (Cameron, 2005; Cameron and Sherrington, 1996; Kimmins and Cameron, 2011; Silverstein, 2014; Zhang and Cooper, 2005). This method is based on the use of highly concentrated reverse emulsion, well-known under the HIPE acronym, for high internal phase emulsion, as template followed by the polymerization of the continuous phase. A HIPE is obtained when the dispersed phase represents more than 64%$_v$ of the sample for a monodisperse emulsion and 71%$_v$ for a polydisperse one. Internal volume fraction of 64%$_v$ corresponds to the random close packing of hard spheres, which means that for higher volume fraction the droplets begin to deform (Cameron and Sherrington, 1996). The resulting materials were first produced and called polyHIPE by Unilever in 1982 (Barby and Haq, 1982) for polymerized High Internal Phase Emulsions. This technique allows easily accessing an open porosity with important interconnected structure (Lépine et al., 2008) (an example of which is shown in Figure S1, SI). PolyHIPE exhibits complex morphologies. They possess cavities, called cells or voids, and pores/holes/windows that interconnect these cells. To stabilize such large volume of internal phase, usually large quantity of surfactant (often up to 30% of the continuous phase) is solubilized in the organic phase (Silverstein, 2014). The main disadvantage when using surfactants is the emulsion stability during the elaboration process. Indeed, as polymerization is often thermally induced and since surfactants have low desorption energies (Leal-Calderon and Schmitt, 2008), heating may be sufficient to enhance desorption provoking evolution of the emulsion drop size distribution during polymerization (Williams et al., 1990; Williams and Wrobleski, 1988). Large amounts of surfactants molecules in the continuous phase that do not take part of the polymerization may also affect polyHIPE properties.

Over the last two decades, the use of particles as stabilizers has increased in polyHIPE formulation (Gurevitch and Silverstein, 2010; Ikem et al., 2011, 2010, 2008; Silverstein, 2014; Vílchez et al., 2011;

Yang et al., 2017). This kind of materials are called Pickering polyHIPE, by extension of the Pickering emulsion denomination. In addition to the increased emulsion stability, with less than 5% of particles upon the monomer content (*i.e*. with respect to the continuous phase), emulsion drop size can also be easily controlled and tuned (Destribats et al., 2012). Nowadays, the most common particles used to stabilize emulsions are inorganic particles (Destribats et al., 2012; Ikem et al., 2010, 2008; Vílchez et al., 2011). Indeed, only few papers report the use of organic particles for HIPE stabilization (Cohen and Silverstein, 2012; Liu et al., 2017; Pang et al., 2018; Yang et al., 2018). Among them, cellulose nanocrystals (CNC) have gained increasing attention in recent years (Capron and Cathala, 2013; Li et al., 2018; Liu et al., 2017; Tang et al., 2017; Tasset et al., 2014; Werner et al., 2019). CNC are particles of growing interest because they are bio sourced, and highly available. They also have very good mechanical properties (Cameron and Sherrington, 1997; Habibi, 2014; Klemm et al., 2011; Lavoine and Bergström, 2017; Tang et al., 2017; Werner et al., 2018), and as demonstrated by Moon et al., they may improve composite properties (Klemm et al., 2011; Postek et al., 2013). One can expect that the addition of CNC in the emulsion formulation might increase the mechanical or optical properties of the final materials. So far, only CNC stabilized-MIPE (Capron and Cathala, 2013) (medium internal phase emulsion, for internal fraction above 50%) and HIPE (Liu et al., 2018) were obtained, and only one attempt of polymerization of the water continuous phase of O/W HIPE was realized (Liu et al., 2017). To our knowledge, no work reported the polymerization of the organic continuous phase of W/O HIPE stabilized by modified CNC.

In previous contribution (Werner et al., 2019), we studied the stabilization of styrene-based direct, inverse and double Pickering emulsions stabilized by CNC modified with appropriate α-bromoisobutyryl rates (CNC-Br) and their polymerization. However, only controlled radical polymerization (AGET SI ATRP) was studied, and no quantitative link between the emulsion characteristics and the polyMIPE properties was reported (in this study the dispersed phase represented 60%, that enters the MIPE designation). Herein we prepared and studied a range of hybrid polymer materials from free radical polymerization of styrene/divinylbenzene Pickering HIPE,

stabilized by modified-CNCs. In a first part, CNC modification for emulsion stabilization is presented. Inverse emulsions stabilization is assessed and parameters varied to obtain different droplet sizes. Then the continuous phase was polymerized leading to porous materials. Finally, the porosity and mechanical properties were studied varying the CNC concentration and water phase content.

2. Experimental

2.1 Materials

Freeze-dried CNC isolated from sulfuric acid hydrolysis (Dong et al., 1998) of wood pulp were purchased from The University of Maine. They present on their surface both sulfate functions (1.05%$_{wt}$ as data from the provider) and surface hydroxyl functions (3.10 ± 0.11 mmol.g^{-1} of CNC (Brand et al., 2017)). The initial CNC had rod-like shape with estimated dimension of 138 ± 47 nm in length and 25 ± 6 nm in width based on AFM analysis (Figure S2, SI).

Styrene (99%, St), Divinylbenzene (80%, DVB), Azobisisobutyronitrile (98%, AIBN), 4-diméthylaminopyridine (99%, DMAP) and sodium chloride (NaCl) were purchased from Sigma Aldrich. α-bromoisobutyryl bromide (98%, Bibb) was purchased from ABCR. Triethylamine (99%, TEA) was purchased from Fisher Scientific. All reagents were used as received without further purification.

2.2 CNC-Br synthesis

CNC-Br synthesis was first described by Zhang et al. (Meng et al., 2009) and Morandi et al. (Morandi et al., 2009) and adapted by Werner (Werner et al., 2019). 1 g of CNC and 1 g of DMAP were introduced in a reaction vessel. After a nitrogen purge, 50 mL of dry DMF were added. The solution was cooled to 0°C thanks to an ice bath and 4.25 g (0.74 mol/L) of Bibb (reactant) and 2.4 g (0.95 mol/L) of TEA, were added to the solution under vigorous agitation. After 72 h of reaction, CNC-Br were precipitated in a mixture of THF/ethanol (50/50$_{v/v}$), isolated by centrifugation (6000 rpm, 10 min, 15°C) and redispersed in water. The crystals were washed several times with a mixture of water/THF/diethyl ether. The final dispersion in water was freeze-dried to obtain a white powder.

The grafting was confirmed by CP MAS NMR (Figure S3, SI) and FT-IR by following the apparition of the stretching bonds corresponding to the sulfate ester groups at 1760 cm^{-1} (v(C=O)) and 1060 cm^{-1} (v(C-O)). The modification rates were evaluated by elemental analysis thanks to the mass percentage of bromine and the amount of surface hydroxyl groups (Equation 1).

$$\%\ substitution = \frac{mmol\ of\ Br\ by\ gram\ of\ CNCs}{mmol\ of\ surface\ hydroxyl\ functions\ by\ gram\ of\ CNCs} = \frac{n_{Br}}{n_{OH}}.100$$

Equation 1

With n_{OH} = 3.10 $mmol.g^{-1}$

2.3 Emulsification and characterization

The organic phase, composed of $50/50_{wt/wt}$ of St/DVB, CNC-Br (from 3 to 20 g/L of dispersed phase) and $1\%_{wt}$ of AIBN was sonicated with a Bioblock vibra-cell equipped with an ultrasonic tip during 1 min (cycles of 1 s "on" at 20% power and 1 s "off"). The aqueous phase, composed of deionized water and sodium chloride (20 mM) was added to the organic phase in order to obtain $60/40_{wt/wt}$ of W/O. These two phases were mixed with a rotor-stator, Ultraturrax©, at 15 000 rpm during 30 seconds in order to obtain a pre-emulsion. Under agitation the aqueous phase was added dropwise to finally reach a ratio of $80/20_{wt/wt}$. These emulsions were characterized by optical microscopy. Because of the toxicity of the St, samples were sealed between two microscope slides before observation. Size distribution was obtained by measuring the diameter of a hundred of drops with ImageJ software. Then the surface average diameter, or Sauter diameter $D_{3,2}$ was calculated following the definition:

$$D_{3,2} = \frac{\sum i\ N_i.D_i^3}{\sum i\ N_i.D_i^2}$$

Equation 2

The surface uniformity was calculated in order to determine the polydispersity of the emulsions, where $\overline{D}$ is the median diameter that is to say the diameter for which the cumulative undersized volume fraction is equal to 50%

125 $$U = \frac{1}{\bar{D}} \cdot \frac{\sum_i |D_i - \bar{D}| \cdot D_i^2}{\sum_i D_i^2}$$

126 *Equation 3*

127 In the following, an emulsion is considered as monodisperse if U is lower than 0.3.

128 **2.4 Polymerization and characterization**

129 Polymerization was carried out in 4 mL vials. The emulsions were heated to 70°C thanks to an oil bath,
130 the reaction was carried out during 24h. At the end of the polymerization, the material was removed
131 from the vial and washed several times with a Soxhlet apparatus, once during 24 h with ethanol and
132 then 6 h with acetone. The final materials were dried at 60°C in an oven. Materials morphology was
133 characterized by Scanning Electron Microscopy (SEM). Similarly to emulsions, Sauter diameter $D_{3,2}$ was
134 obtained with ImageJ software by measuring a hundred cells. Samples porosity was assessed by
135 mercury intrusion porosimetry. Mechanical properties were evaluated by extracting the compressive
136 modulus by Dynamic Mechanical Analysis (DMA).

137 **Instrumentation**

138 Infrared spectra of unmodified and brominated CNC were recorded using a Vertex 70 Bruker FT-IR
139 spectrometer. CNC powder was analyzed thanks to an attenuated total reflectance ATR accessory.
140 Each spectrum was recorded between 4000 cm^{-1} and 400 cm^{-1} with a resolution of 4 cm^{-1} with 32 scans.

141 Materials morphology was characterized with SEM TM-1000 with acceleration voltage of 15 kV. The
142 samples were stick onto support with silver lacquer and metallized with gold/palladium coating during
143 60 seconds. Slice of materials (70 nm) were obtained by cryo-ultramicrotomy with a Leica UC7 at -90°C
144 and were observed at ambient temperature with a TEM Hitachi H7650.

145 The experimental porosity of the samples was determined by mercury intrusion porosimetry in a
146 Micromeritics Autopore IV 9500 porosimeter with the following parameters: contact angle = 130°,
147 mercury surface tension = 485 mN m^{-1}, maximum intrusion pressure = 124 MPa. The analysis was
148 replicated at least 3 times for each set of parameters.

A TA Instrument RSA3 (dynamic mechanical analysis, DMA) was used to study the mechanical properties of the samples, with a cylindrical shape of 20 mm diameter of 7.5 ± 1.5 mm thick. The compression test was performed in static mode at ambient temperature, during 10 s at a rate of 1mm/s until a force of 35 N is reached. Each set of experiments was replicated 5 times to insure the reproducibility of the analysis.

3 Results and discussion

3.1 CNC modification

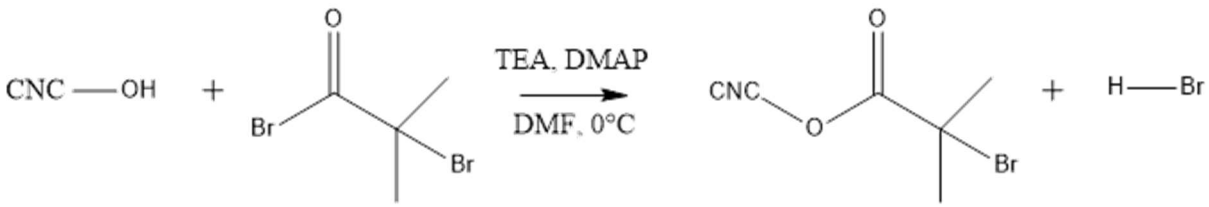

Figure 1: CNC modification scheme

Because of surface hydroxyl functions, CNC are mainly hydrophilic. One big advantage is that this surface is easily tuneable and new reactive functions can be grafted, by oxidation, carbamation, etherification or by esterification (Eyley and Thielemans, 2014). Esterification reaction is known to be fast and to offer a wide range of graft possibilities, therefore, this reaction was used in the following to graft Bibb function onto the CNC surface in order to modify the hydrophobic/hydrophilic balance of the CNC (Figure 1). The use of Bibb allows providing hydrophobicity. In addition it may be useful as polymerization initiator (Meng et al., 2009; Morandi et al., 2009; Werner et al., 2019). As described by Werner et al. (Werner et al., 2019), the highest grafting ratio was targeted so that the crystals would present interfacial properties, and therefore could be used as inverse emulsion stabilizers (Figure S4, SI). Bromine mass percentage was determined by elemental analysis (26%wt) and thanks to the initial number of surface hydroxyl functions (3.10 mmol/g of CNC), a substitution rate of 105% could be extracted using Equation 1. Because of the material variability, initial amount of hydroxyl function was eventually underestimated and therefore, substitution rate was overestimated. Further

characterization of the resulting crystals in terms of chemical modification and morphology is provided in SI (Figures S3, S5 and S6, SI).

3.2 Emulsions formulation

3.2.1 High internal phase emulsion preparation

The continuous organic phase of the inverse emulsions was composed of styrene and DVB and the aqueous dispersed phase was composed of salted water (20 mM NaCl) ; these emulsions were stabilized by the 100% modified CNC-Br, presented previously. We chose the most commonly studied St/DVB system for polyHIPE synthesis (Cameron et al., 1996; Cameron and Sherrington, 1997; Ceglia et al., 2012; Hainey et al., 1991; Ikem et al., 2011) in order to have a polymer matrix of reference. To obtain HIPE, volume fraction of internal phase was set above 64%$_v$ the random close packing of monodisperse emulsions. More precisely, a W/O volume ratio of 79/21$_{v/v}$ was chosen (equivalent to a 80/20$_{wt/wt}$), this fraction corresponds to the highest water content we could easily achieve. However, more concentrated emulsions were obtained by centrifugation and removal of the organic supernatant. The maximal ratio reached with this technique without destabilization under centrifugation was 83/17$_{v/v}$.

Given the substitution rate of the CNC-Br, their aggregation make them difficult to redisperse in the organic phase. As sonication is expected to improve dispersion of the CNC-Br in the organic phase, two emulsions have been prepared: one with and the other without preliminary sonication of the CNC-Br suspension.

Without sonication, the mean drop diameter was above 200 µm, whereas after sonication the drop size was divided by a factor 2, around 100 µm (Figure S7, SI). This result shows that a better dispersion of the CNC-Br leads to a better availability of the crystals resulting in a higher stabilizing efficiency; a larger interfacial area can be stabilized, hence the drops diameter decreases. As a consequence in the following, all the emulsions were prepared with prior sonication of the CNCBr in the organic phase.

3.2.2 Influence of CNC-Br concentration on droplets diameter

Emulsions were successfully prepared using different concentrations of CNC-Br in the range 3 g/L – 20 g/L with respect to the dispersed phase. The water volume fraction of $79/21_{v/v}$ was kept constant. The droplet diameter varies with the CNC-Br concentration. The plot of $1/D_{3,2}$ versus the concentration of CNC-Br showed a linear dependence between the two parameters which is consistent with the limited coalescence phenomenon occurring for Pickering emulsions in the case of irreversible particle adsorption and in the particle-poor domain(Arditty et al., 2003; Wiley, 1954) (Figure S8, SI). Indeed, the higher CNC-Br concentration, the larger amount of stabilized interfacial area and thus the lower the droplet diameter. In this linear domain, emulsion size is controlled by the amount of particles and the way they pack at the interface. A relative narrow drops size distribution width is another characteristic of this domain (U≈ 0.3).

From the slope, the C parameter was extracted thanks to the following relation(Schmitt et al., 2014):

$$\frac{1}{D_{3,2}} = \frac{m_p}{6.\rho_p.V_d.C}.\frac{a_p}{v_p}$$

Equation 4

where m_p corresponds to the mass of particles, ρ_p their density (taken as 1.6 g/cm^3), a_p and v_p the surface and volume of the particles in contact with the interface (calculated for a crystal of dimension 140x25x25 nm^3) , V_d the volume of the dispersed phase, and C the covering ratio.

The C parameter is defined as the proportion of the interface that is covered by particles. Given the almost rectangle parallelepiped shape of the particles, for a dense monolayer this parameter would be equal to 1. If C > 1, then multi-layers are present at the interface and the number of layers n can be estimated through: C = n x 100%. In the present case, C ≈ 5, which means there are in average 5 layers of CNC-Br on the droplets surface.

3.3 Emulsions polymerization

3.3.1 Study of a reference polyHIPE

The reference emulsion was composed of 79/21$_{v/v}$ of W/O ratio, 50/50$_{wt/wt}$ of St/DVB ratio, 8 g/L of CNC-Br with respect to the dispersed phase. The Inverse emulsion was characterized 1 hour after emulsification and remained stable for at least two days (Figure S9). Porous material was obtained after free radical polymerization of the continuous phase by heating the HIPE at 70°C for 24 h. The obtained material was white and cohesive forming a self-standing monolith (Figure S10, SI). Furthermore, polymerization showed a good conversion of 85%. The conversion was obtained by gravimetric measurement of the monolith, by measuring the monolith weight after washing and drying and comparing it to the initial mass of the organic phase containing the monomers.

Comparison of the emulsion before and after polymerization showed that no destabilization occurred during the process. Indeed, cells were clearly observed by SEM with diameter matching the original emulsion drop sized obtained by optical microscopy. Comparison between the emulsion and the polyHIPE (Figure 2) revealed identical sizes within error, between the emulsion droplets 122 ± 23 µm, and the polyHIPE cell size 125 ± 37 µm (Table 2, sample PPH-1). The good agreement between drop and cell sizes and the absence of fracture in the monolith also indicates that no coalescence neither contraction occurred during polymerization.

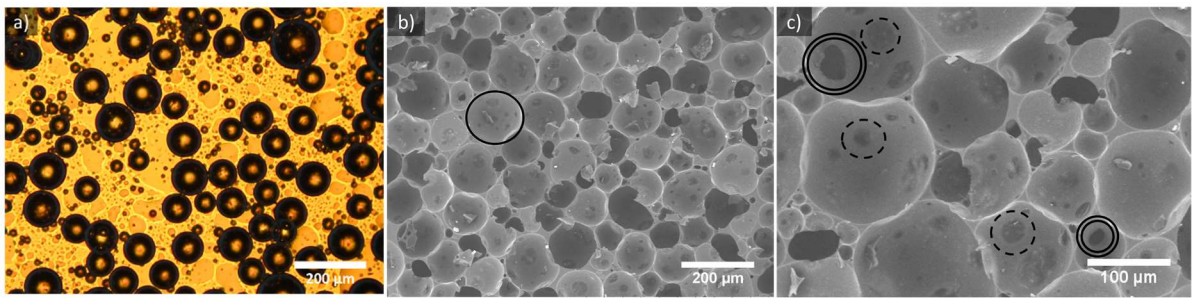

Figure 2: a) Microscopic pictures 79/21$_{v/v}$ HIPE, with 10 g/L of CNCBr with respect to the aqueous phase with sonication, diluted, b) c) SEM pictures of corresponding solid dried material with the cell (straight line), open pores (double line) and closed pores (dashed line)

The morphology of the obtained polyHIPE (Figure 2) differs from usual open-cell polyHIPE stabilized by surfactant, but seems typical for a particle-stabilized Pickering polyHIPE. Indeed, conventional polyHIPE stabilized by surfactant and particle-stabilized Pickering polyHIPE present different types and aspects of porosity. The first category of polyHIPE usually presents an obvious open-cell structure with well-

242 defined pores. A large number of paper has been devoted to the study of structure-properties
243 relationship of these porous materials among which the mechanism of the pore formation in polyHIPE.
244 The hypothesis that pores result of the cracking of polymer film during the purification process
245 (Cameron et al., 1996) was ruled out thanks to Gilti et al. (Gitli and Silverstein, 2008). The most common
246 explanations are that the formation of the cells interconnections is due to mechanical rupture of the
247 polymer film during the polymerization step (Menner and Bismarck, 2006; Williams and Wrobleski,
248 1988) where the water droplets are the closest and the polymer the thinnest, which can be supported
249 by Ceglia et al. work showing a very good adequacy between the dimension of the liquid film separating
250 two emulsion drops (that depends on the drops size and the dispersed phase volume fraction) and the
251 size of the interconnexions (Ceglia et al., 2012). Alternatively, for Barby and coll. (Barby and Haq, 1982)
252 the formation of pores is due to the removal of surfactant from the two emulsion phases during the
253 washing step (Lépine et al., 2008). Finally, Stubenrauch and Drenckan also discussed the role of the
254 initiator locus in the pore formation for surfactant stabilized polyHIPE showing an influence of the
255 phase in which it is solubilized (Quell et al., 2016). With regards to Pickering polyHIPE, Cameron et al.
256 explained that the monomer contraction during polymerization was restricted to the gel point so that
257 a film would be formed instead of an open pore, which could eventually rupture submitted to vacuum
258 process (Kimmins and Cameron, 2011). Therefore, for organic Pickering polyHIPE no open-cell
259 structure was evidenced so far (Ikem et al., 2010, 2008; Menner et al., 2007a, 2007b), but some
260 attempts to produce an open-cell structure were realized by adding small amounts of non-ionic
261 surfactant as co-stabilizer (Ikem et al., 2011).

262 Therefore, it was not surprising observing in our samples some open pores (dotted line), but mostly
263 pores covered by a thin polymeric film (Figure 2 dashed lines). In order to assess the closed or open
264 structure of the polyHIPE, one can compare the monolith density also given by mercury intrusion
265 porosimetry and the one estimated either through the mass to volume ratio of the macroscopic
266 monolith or estimated from the monolith composition. In the later calculus, the density of
267 poly(styrene-DVB) has been taken equal to 1.06 g/cm^3, density of CNC as 1.6 g/cm^3 and for different

monomers conversions (Figure S11, SI). The estimated porosity from the composition was taken equal to the initial volume fraction of water within the HIPE. The porosity estimated from the mass to volume ratio was deduced from the as-measured density in comparison with the density of the matrix composed of styrene, DVB and CNC. All three set of density and porosity were compared (Table 1).

	Density (g/cm^3)	Porosity (%)
Estimated from the composition (100% conversion)	0.21	79
Estimated from the composition (85% conversion)	0.18	
Estimated from the mass to volume ratio	0.12	88
Mercury porosimetry measurement	0.18	81 ± 2

Table 1: Features estimated and measured by porosimetry of reference polyHIPE

Estimated values of density and porosity are very close to the measured ones especially those issuing from the composition taking into account the 85% conversion of the monomer. Values from the mass to volume ratio are a bit different probably due to a lack of precision of the way measuring the volume. The good agreement indicates that the whole monolith is accessible therefore that the porosity is open. This was verified with the full data given by the mercury porosimetry analysis, plotting the mercury intrusion as a function of the pressure (Figure 4). Two ranges of mercury intrusion were identified from Figure 4 a-b, one at low pressure, around 0.02 MPa and another around 2 MPa. This observation is in agreement with the hypothesis of a double population of holes: one corresponding to holes easily accessible to mercury, and the other more difficult to access. Through Washburn equation, pores diameter can be obtained from mercury pressure values, Equation 5:

$$D = -(\frac{1}{P})\ 4.\gamma.\cos\varphi$$

Equation 5

where D is the hole diameter, P the mercury pressure, γ the surface tension of the mercury (taken equal to 485 mN/m) and φ the wettability angle of mercury (130°).

Intrusion at low pressure was attributed to large pore sizes (110 µm) (Figure 4 b), corresponding to the cells of the polyHIPE (125 µm). At higher pressures, a second population of holes (< 1 µm) with a much

higher mercury intrusion value was identified though difficult to observe by SEM and showed to be responsible for the open porosity of the material (Figure 4 a). However, if the second pore population would directly result from the contact films between the drops one would expect holes between the cells with 39 µm in diameter for 79%$_v$ (see Figure S12 (Ceglia et al., 2012)). These values are far from the measured ones around 0.66 µm. This seems indicating either that CNC-Br induce a repulsion at a much larger scale that the thickness of 5 CNC layers between the drops or that the interconnections do not results from the contact zones between initial drops. The presence of this second smaller population of pores is in agreement and supports the hypothesis made by Silverstein et al. (Gurevitch and Silverstein, 2010), for polyHIPE stabilized with silica nanoparticles, believing in the existence of an interconnectivity within Pickering polyHIPE at a smaller scale in spite of a seemingly closed-cell structure. As for the described materials, the polyHIPE presented here were easily washed and dried, the ability to easily remove water being another argument in favor of an open-cell structure (Gurevitch and Silverstein, 2010). It is worth noticing here that washing and drying were performed in mild conditions (avoiding use of vacuum) to avoid any material structure modification. Furthermore, as the majority of the porosity was accessed at high pressure above 1 MPa, and given the mechanical strength of the polymer which should have undergone breakage below 1MPa, it was assumed that no breakage of the solid foam occurred during the mercury porosimetry analysis, validating the open porosity conclusion.

The mechanical properties of polyHIPE were studied by compression measurements at room temperature. Compressive moduli (that we'll call Young modulus even if the experiments were not performed under traction) were extracted from the slope of the linear region of the stress-strain curve (Figure S13, SI). Three different domains were identified: the linear domain, where the deformation was reversible and from which the modulus was extracted, the plateau and the densification domains, where the material fell apart. The compression modulus for the reference monolith reached 2 MPa, which was lower than expected for polyHIPE reinforced with particles. Typical values of compressive moduli for St/DVB polyHIPE stabilized by surfactants were estimated around 10 MPa (Gitli and

315 Silverstein, 2008; Tai et al., 2001) and Pickering polyHIPE stabilized solely with titania nanoparticles
316 showed an enhancement of the compressive modulus up to 65 MPa in similar conditions. The low
317 compressive modulus found for CNC-stabilized polyHIPE was surprising, given the high aspect ratio and
318 strength of the CNC (Klemm et al., 2011; Tang et al., 2017). However, successful reinforcement
319 required homogeneous repartition of the fillers, with adhesion of the particles to the matrix which was
320 likely not the case for the studied system since CNC-Br were not reactive and accumulated at the
321 interface (forming 5 layers around the drops). This corroborates the hypothesis of Bismarck et al. when
322 they proposed that particles agglomerate at the interface acts as flaws instead of reinforcing the
323 polymer matrix (Ikem et al., 2010).

324 **3.3.2 CNC-Br concentration impact at fixed water/organic phase ratio**

325 The influence of the cell size was studied by varying the CNC-Br concentration. Four concentrations of
326 CNC-Br were tested: 5 g/L, 8 g/L, 12 g/L and 16 g/L with respect to the dispersed phase keeping all
327 other parameters constant. First, emulsion size was preserved after polymerization (Figure 3 left). At
328 lower CNC-Br concentration, no destabilization phenomenon was observed (coagulum, demixing…)
329 upon polymerization, however drops diameter differed from cells diameter. This deviation from the
330 slope y=x might be explained by deformed SEM pictures harder to analyze (Figure 3 a).

331 Successful materials were synthesized based on these emulsions and characterized by SEM (Figure 3
332 a-d). All the materials were homogeneous regarding their cell size distribution, with a decrease of the
333 cell diameter with the concentration of CNC-Br (Table 2) as expected according to the limited
334 coalescence phenomenon. Each sample exhibited also the presence of pores between the cells
335 covered with polymeric films as discussed previously.

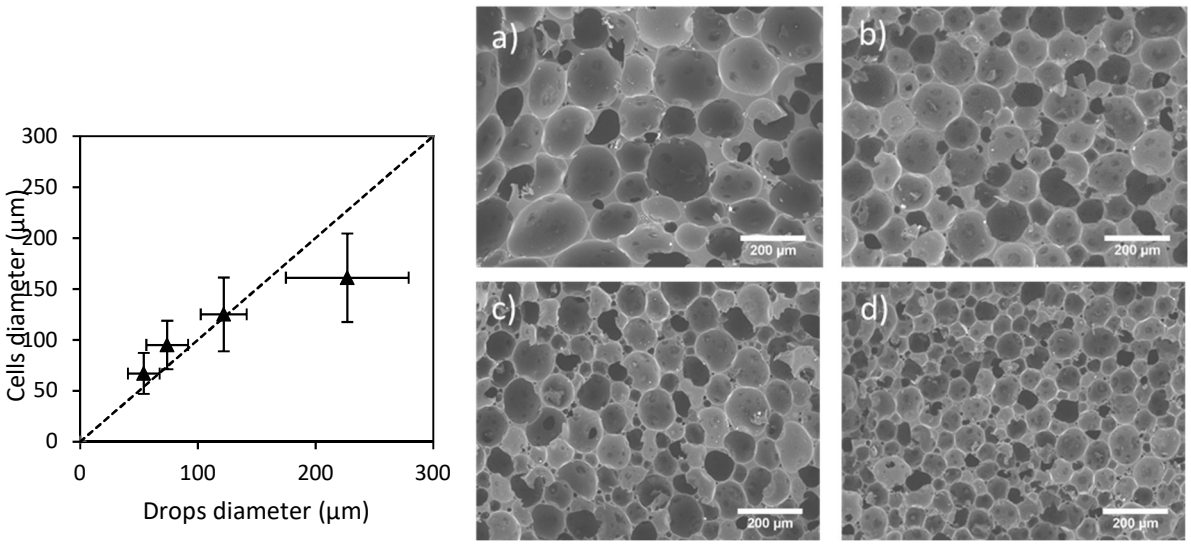

Figure 3: Left, Evolution of the foam cell size determined from SEM observations, as a function of initial water drops size determined by optical microscopy. The dashed line with slope of 1 corresponding to equality is plotted as a guide to the eye. Right, Scanning Electron Micrographs of the final obtained monoliths after washing and drying with initially a) 5 g/L of CNC-Br b) 8 g/L of CNC-Br c) 12 g/L of CNC-Br and d) 16 g/L of CNC-Br with respect to the organic phase

sample	Water/oil wt/wt ratio	Equivalent v/v ratio	[CNC] (g/L)	$D_{3,2}$ HIPE (µm)	$D_{3,2}$ polyHIPE (µm)	Secondary pores diameter (µm)	Porosity (%)	Foam density (g/cm³)	Skeletal density (g/cm³)	E (MPa)
PPH-1	80/20	$79/21_{v/v}$	8	122 ± 23	125 ± 37	0.66	81 ± 2	0.18	0.97	2.05 ± 0.19
PPH-2	80/20	$79/21_{v/v}$	5	227 ± 53	164 ± 39	0.74	79 ± 2	0.19	0.93	1.68 ± 0.21
PPH-3	80/20	$79/21_{v/v}$	12	74 ± 18	95 ± 23	0.57	80 ± 2	0.20	0.98	1.94 ± 0.09
PPH-4	80/20	$79/21_{v/v}$	16	54 ± 14	67 ± 22	0.55	80 ± 2	0.19	0.94	1.79 ± 0.24

Table 2: PolyHIPE characteristics varying the CNCBr concentration

Mercury intrusion porosimetry results were consistent with an open-cell structure for all CNC-Br concentrations as it was shown for the reference polyHIPE sample (Figure 4 a-b). Two populations of holes were identified: the largest corresponding to the cells and a second one smaller, corresponding to a much higher mercury intrusion pressure, similarly to the reference sample, and suggested to be responsible for the overall interconnectivity. Interestingly, the second population diameter decreases with increasing amount of CNC-Br used to stabilize the polyHIPE (Table 2) at constant drop coverage by the particles (since the samples belong to the limited coalescence domain where the coverage is constant).

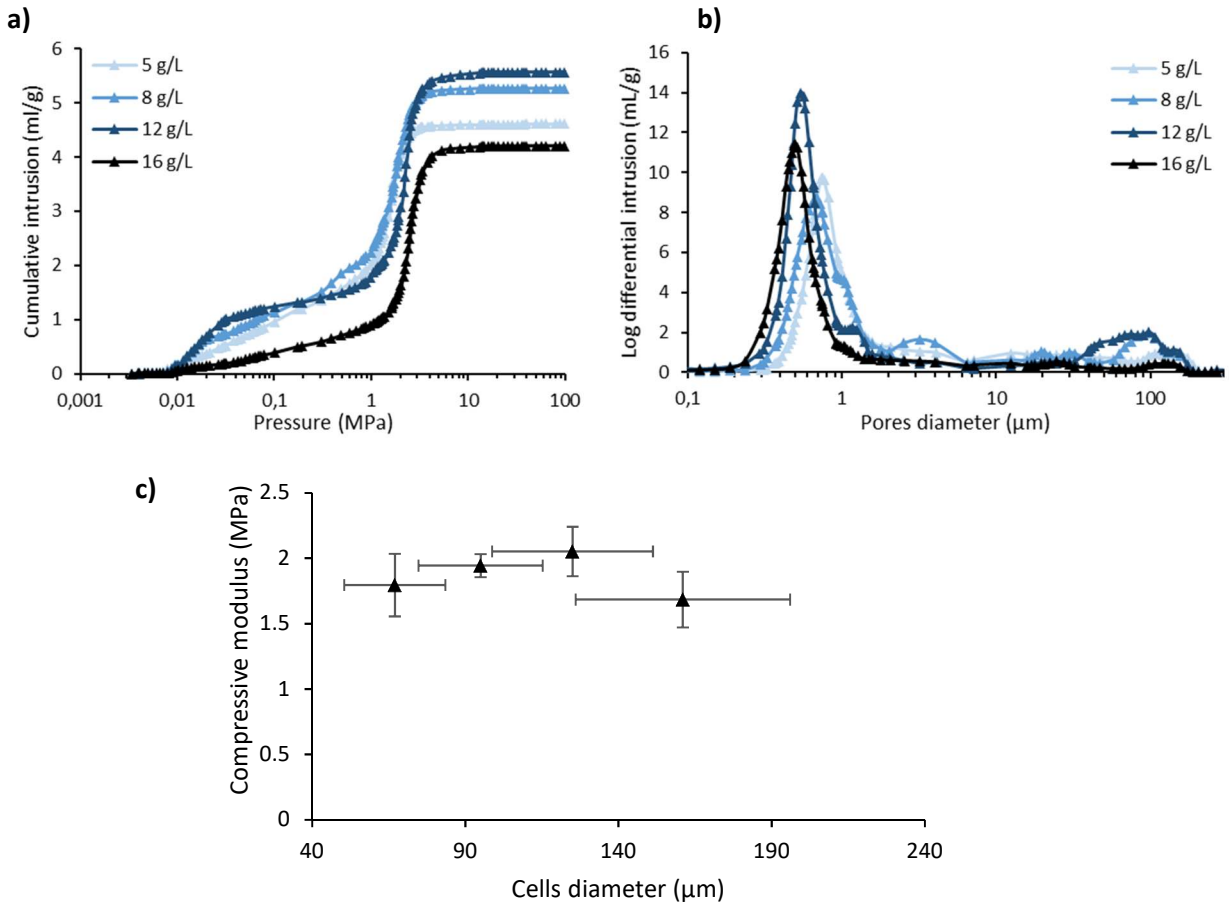

Figure 4: a) b) Mercury intrusion as function of pores diameter for different size diameter, c) compressive modulus of porous materials as function of cells diameter

Mechanical analyses were performed on the four samples and compressive moduli were extracted. As shown in Figure 4 c, there was no significant difference between the four samples, the moduli varying in the range 1.5 MPa – 2 MPa. As a result, no dependence of the modulus with the cell size was assessed for these porous materials. This behaviour was expected, and even predicted by the Gibson and Ashby model (Gibson and Ashby, 2014), which is often used to describe polyHIPE behaviour (Gibson and Ashby, 2014). This model states that the elastic modulus does not depend on the cell size, but only varies with the fraction of continuous phase which is here kept constant. This model is based on the double hypothesis that the material has an open porosity and is homogeneous, and the lack of one implies deviation from the model as it was observed by Ceglia et al. with polyHIPE stabilized by surfactants (Ceglia et al., 2012). First hypothesis was verified by previously described mercury intrusion porosimetry analysis. Concerning the homogeneity of the matrix, this hypothesis was verified by cryo-

TEM observations of 70 nm thick slices cut in the material. Cryo-TEM pictures showed a homogeneous polymer matrix even at low scale (see Figure S14, SI).

Contrary to surfactants, the concentration of CNC-Br did not show any influence over the interconnectivity of the polyHIPE or the mechanical properties of the sample. Even samples with low concentration of CNC-Br (5 g/L) did present an open-cell structure, which remained at high concentration (16 g/L). The increase in stabilizer concentration neither did affect the global structure of the formed material, since self-standing monoliths were produced for all concentrations contrary to what was observed by Williams and Wrobleski (Williams and Wrobleski, 1988) for polyHIPE stabilized with sorbitan monoleate. As it was explained for the reference polyHIPE sample, no improvement of the mechanical properties was obtained by the presence of CNC-Br nor by increasing the particle content in this range of concentration (Figure 4 c). But yet, the increase of particle content did not reduce the young modulus as it was observed for titania nanoparticles (Ikem et al., 2010).

3.3.3 W/O ratio impact at a fixed drop size

From the Gibson and Ashby model, the foam fraction or continuous phase fraction is expected to influence the polyHIPE properties following Equation 6 (Ceglia et al., 2012).

$$\frac{E^*}{E_s} \propto \left(\frac{\rho^*}{\rho_s}\right)^2 = \left(1 - \phi_{foam}\right)^2$$

Equation 6

Where E* and ρ* are respectively the compressive modulus and the density of the polyHIPE, E_s and ρ_s respectively the Young's modulus and the density of the material constituting the solid (poly(styrene-co-divinylbenzene)) and ϕ_{foam} the foam volume fraction or equivalently the water volume fraction of the initial emulsion as no contradiction was observed. E_s is taken as 500 GPa as reported in the literature for similar polymers (Ceglia et al., 2014; Graeber, 2013).

Here, the study focused on three distinct ratios, keeping a water volume fraction above 64%$_v$ to remain in the HIPE denomination: 74/26$_{v/v}$, 79/21$_{v/v}$ and 83/17$_{v/v}$. As the amount of CNC-Br determines the

drop size, we chose to maintain the ratio of the amount of CNC-Br to the amount of dispersed phase constant (see Equation 4). This value is fixed at a value of 8 g/L with regards to the dispersed phase for all samples. After optical observation, the droplets diameter was measured to be around 125 µm for all three formulations (Table 3). The last ratio ($83/17_{v/v}$) was reached thanks to centrifugation of the emulsion and removal of the organic supernatant.

sample	Water/oil wt/wt ratio	Equivalent v/v ratio	[CNC] (g/L)	$D_{3,2}$ HIPE (µm)	$D_{3,2}$ polyHIPE (µm)	Secondary pores diameter (µm)	Porosity (%)	Foam density (g/cm^3)	Skeletal density (g/cm^3)	E (MPa)
PPH-1	$80/20_{wt/wt}$	$79/21_{v/v}$	8	122 ± 23	125 ± 37	0.66	81 ± 2	0.18	0.97	2.05 ± 0.19
PPH-5	$75/25_{wt/wt}$	$74/26_{v/v}$	8	120 ± 25	122 ± 36	0.50	75 ± 2	0.24	0.96	2.08 ± 0.31
PPH-6	$85/15_{wt/wt}$	$83/17_{v/v}$	8	150 ± 38	127 ± 34	1.22	85 ± 2	0.12	0.81	1.48 ± 0.36

Table 3: PolyHIPE characteristics varying the W/O fraction

As previously noticed, homogeneous self-standing monoliths were obtained, but SEM micrographs (Figure 5) revealed an inner structural difference. As expected, when the volume of water increased, the polyHIPE cells deformation increased until to reach almost polyhedral shapes. This evolution originates form the higher packing of the drops, leading to an increase of the contact surface between two adjacent cells, as can be seen from Figure 5, forming larger interconnections.

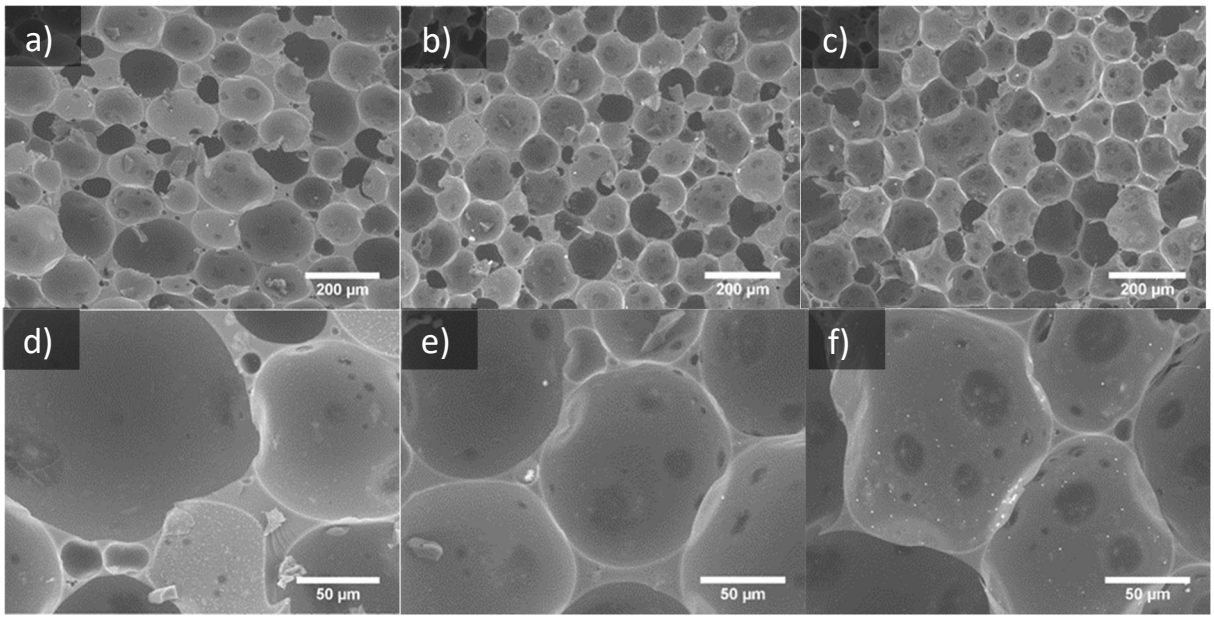

Figure 5: Scanning Electron Micrographs of the solid dried material with ratio W/O of a) $74/26_{v/v}$ b) $79/21_{v/v}$ and c) $83/17_{v/v}$ and d) e) f) respective zoom into the cells

These observations were verified by mercury intrusion porosimetry (Figure 6 a-b). As previously observed samples showed a double population of holes, one with larger diameters resulting from the emulsion droplets, and another at a smaller scale. As expected, porosity increased with the water volume fraction, with good adequacy between initial emulsion composition and porosimetry measurements (Table 3). When the water volume fraction increased the mercury intrusion into the sample was facilitated. This phenomenon was mainly observed as intrusion pressure decreased, shifting the small holes population diameter towards larger values. These results were in good adequacy with the observation made by SEM (Figure 5). Indeed, Figure 5 shows the presence of larger holes in samples with higher water volume fractions: 1.2 µm for the highest water content ($84/16_{v/v}$), decreasing to 0.7 µm for the intermediate water content ($79/21_{v/v}$) reaching 0.5 µm for the smallest water volume fraction ($74/26_{v/v}$).

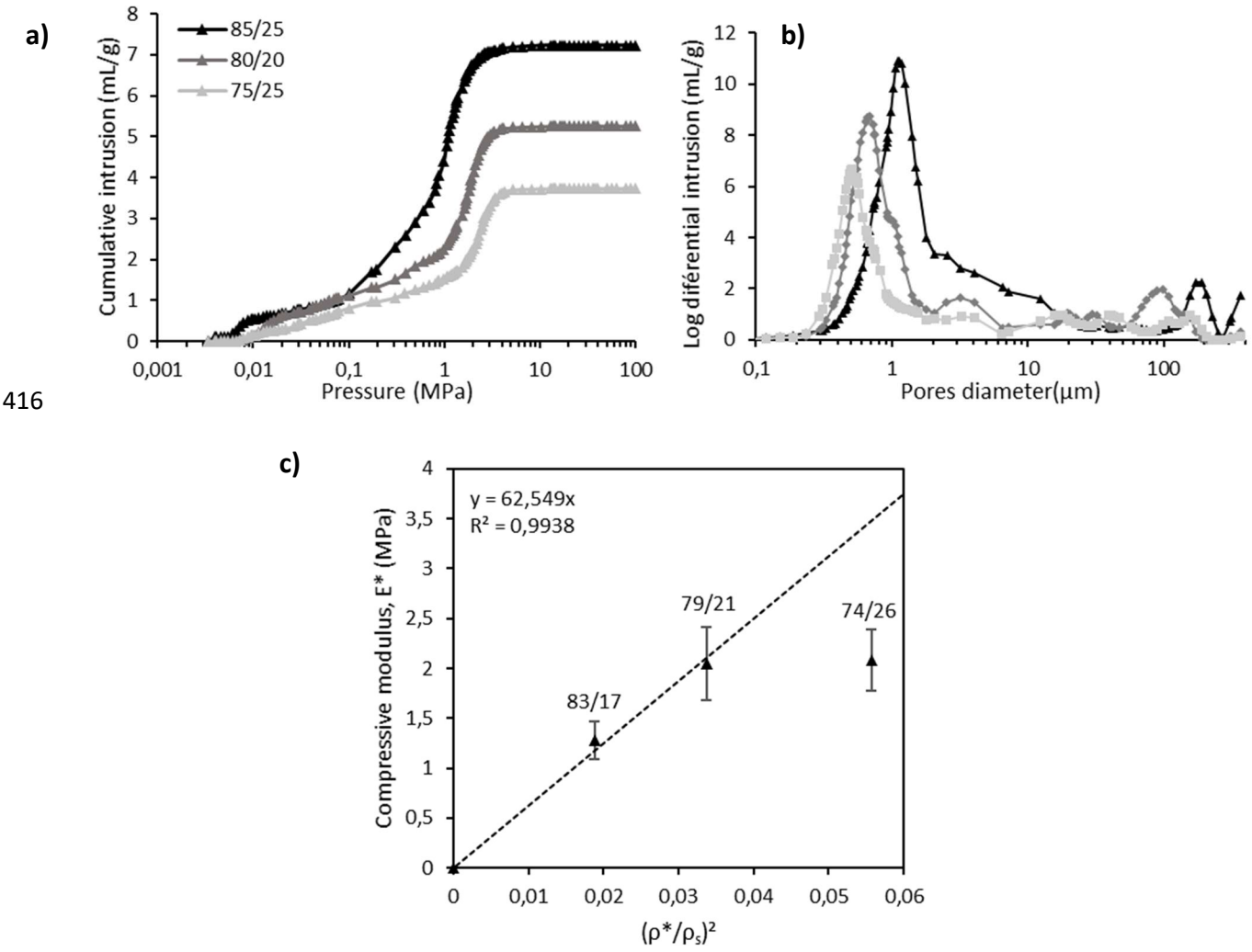

Figure 6: a) b) Mercury intrusion as function of pores diameter for different W/O ratio, c) Compressive modulus evolution with relative density (Gibson and Ashby model prediction in dotted line)

Mechanical analysis were performed and the compressive moduli were extracted. As described by Equation 6, the compressive modulus was plotted against the square of the relative density (Figure 6 c), and showed a linear dependence according to Equation 6. However, a deviation can be observed at the lowest studied water volume fraction (highest density). Several explanations could be proposed to explain this behaviour: at least one of the two hypothesis of the Gibson and Ashby model might not be verified anymore. The open-porosity hypothesis was verified by mercury intrusion porosimetry, therefore rather questioning the homogeneity of the matrix. Indeed, cell-to-cell wall thickness increases with decreasing water content, the localisation of the CNC-Br at the interface might induce

a non-negligible inhomogeneous composition of the wall. This hypothesis was confirmed by a closer look at SEM microcrographs of samples PPH-5 (74/26$_{v/v}$) and PPH-6 (83/17$_{v/v}$), Figure 7 .

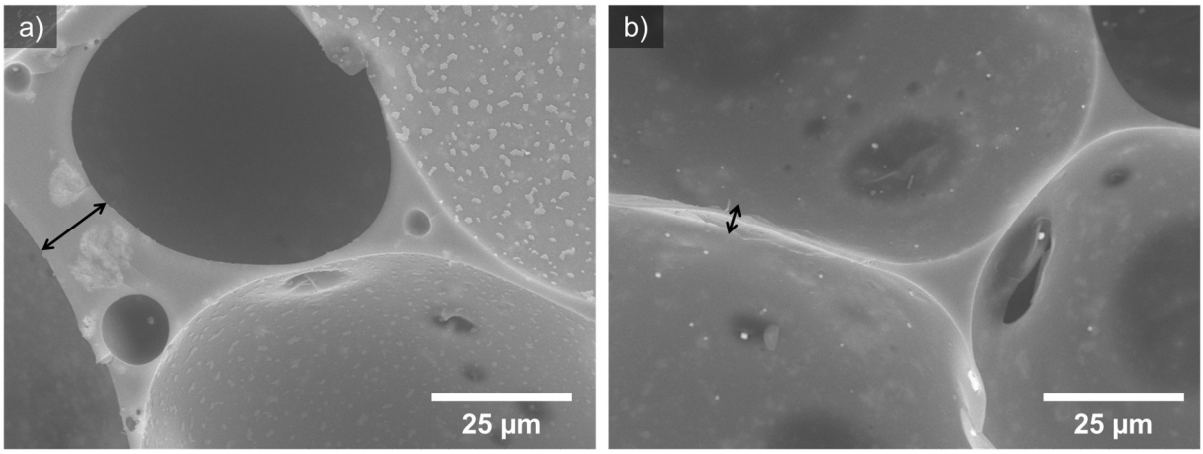

Figure 7: Impact of W/O ratio on polymer film (continuous line), (a) for low water ratio 74/26$_{v/v}$ and (b) for high water ratio 83/17$_{v/v}$

Thickness of polymer films were measured and the results are compared to the estimated thickness of the CNC-Br envelope present at each cell surface. Given the fact that an average of 5 layers of CNC-Br was calculated to be present at each cell surface, a minimum of 125 nm is to be considered for a dense packing of the rods. Therefore, a homogeneous polymer matrix could only be assumed if the polymer film thickness does not exceed 250 nm, maximal value when two CNC-Br envelopes of neighbouring cells come into contact. The film thickness deduced from the SEM picture in the case of the highest concentrated emulsion-base polyHIPE PPH-6 (83/17$_{v/v}$) was about 609 nm, which is of the same order of magnitude (factor 2.4) as the double CNC-Br envelop, while the film thickness of the polyHIPE issuing from the emulsion with the lowest water content PPH-5 (74/26$_{v/v}$) was measured about 2094 µm which is one order of magnitude larger than this double envelope size. Therefore, we think that the polymeric matrix of PPH-5 (74/26$_{v/v}$) cannot be assumed homogeneous enough to fit in Gibson and Ashby model, contrary to the two other samples.

Conclusion

We have shown in the current paper that cellulose nanocrystals modified with a hydrophobic function (CNC-Br) could stabilize High internal phase emulsions (W/O) with water content of 80%$_{wt}$ that could be easily polymerized to promote materials with an open porosity. Indeed, The HIPE were effectively polymerized without destabilization, and polyHIPE reflected the original HIPE as measured emulsion and cell size were identical. All materials synthesized showed an open porosity, confirmed by mercury intrusion porosimetry analysis and by the fact that all the water caught was evaporated without the use of vacuum and lead to adequate density. Using the limited coalescence phenomenon, monoliths with a wide range of cell diameters were synthesized with both constant density and CNC-Br coverage of 5 layers. Emulsion drop size showed to have no influence over the Young modulus, as predicted by Gibson and Ashby model for porous materials. The use of the model was made possible as the material had an open porosity and by verifying the homogeneity of the polymer matrix by cryo-TEM observation. Also, variation of the density by changing the volume fraction at fixed drop size showed a good dependence of the Young modulus except for high densities. This behaviour was explained by increasing film thickness in-between adjacent cells questioning the matrix homogeneity necessary to apply Gibson and Ashby model. In general, the pore diameter didn't match the calculation made for interconnections resulting from the contact zones between cells. The presence of smaller pores than expected could be explained by the existence of especially thick films.

Aknowledgements

The authors would like to thank the French "Fondation Bordeaux Université" and the "Fonds Ernest Solvay" supported by "Fondation Roi Baudouin" for their financial support.

The authors would like to thank Isabelle Ly for her help in ultramicrotomy and observation of the samples in Cryo-TEM, Eric Laurichesse and Cédric Le Coz for the mechanical analysis using DMA.

References

Arditty, S., Whitby, C.P., Binks, B.P., Schmitt, V., Leal-Calderon, F., 2003. Some general features of limited coalescence in solid-stabilized emulsions. Eur. Phys. J. E 11, 273–281. https://doi.org/10.1140/epje/i2003-10018-6

Barby, D., Haq, Z., 1982. Low density porous cross-linked polymeric materials and their preparation and use as carriers for included liquids. 0,060,138.

Bhumgara, Z., 1995. Polyhipe foam materials as filtration media. Filtration & Separation 32, 245–251. https://doi.org/10.1016/S0015-1882(97)84048-7

Brand, J., Pecastaings, G., Sèbe, G., 2017. A versatile method for the surface tailoring of cellulose nanocrystal building blocks by acylation with functional vinyl esters. Carbohydrate Polymers 169, 189–197. https://doi.org/10.1016/j.carbpol.2017.03.077

Cameron, N.R., 2005. High internal phase emulsion templating as a route to well-defined porous polymers. Polymer 46, 1439–1449. https://doi.org/10.1016/j.polymer.2004.11.097

Cameron, N.R., Sherrington, D.C., 1997. Preparation and glass transition temperatures of elastomeric PolyHIPE materials. J. Mater. Chem. 7, 2209–2212. https://doi.org/10.1039/a702030i

Cameron, N.R., Sherrington, D.C., 1996. High internal phase emulsions (HIPEs) — Structure, properties and use in polymer preparation, in: Biopolymers Liquid Crystalline Polymers Phase Emulsion. Springer Berlin Heidelberg, Berlin, Heidelberg, pp. 163–214. https://doi.org/10.1007/3-540-60484-7_4

Cameron, N.R., Sherrington, D.C., Albiston, L., Gregory, D.P., 1996. Study of the formation of the open-cellular morphology of poly(styrene/divinylbenzene) polyHIPE materials by cryo-SEM. Colloid Polym Sci 274, 592–595. https://doi.org/10.1007/BF00655236

Capron, I., Cathala, B., 2013. Surfactant-Free High Internal Phase Emulsions Stabilized by Cellulose Nanocrystals. Biomacromolecules 14, 291–296. https://doi.org/10.1021/bm301871k

Ceglia, G., Mahéo, L., Viot, P., Bernard, D., Chirazi, A., Ly, I., Mondain-Monval, O., Schmitt, V., 2012. Formulation and mechanical properties of emulsion-based model polymer foams. Eur. Phys. J. E 35, 31. https://doi.org/10.1140/epje/i2012-12031-0

Ceglia, G., Merlin, A., Viot, P., Schmitt, V., Mondain-Monval, O., 2014. Porous materials with tunable mechanical properties. J Porous Mater 21, 903–912. https://doi.org/10.1007/s10934-014-9831-6

Cohen, N., Silverstein, M.S., 2012. One-Pot Emulsion-Templated Synthesis of an Elastomer-Filled Hydrogel Framework. Macromolecules 45, 1612–1621. https://doi.org/10.1021/ma2027337

Destribats, M., Faure, B., Birot, M., Babot, O., Schmitt, V., Backov, R., 2012. Tailored Silica Macrocellular Foams: Combining Limited Coalescence-Based Pickering Emulsion and Sol-Gel Process. Adv. Funct. Mater. 22, 2642–2654. https://doi.org/10.1002/adfm.201102564

Dong, X.M., Revol, J.-F., Gray, D.G., 1998. Effect of microcrystallite preparation conditions on the formation of colloid crystals of cellulose. Cellulose 5, 19–32. https://doi.org/10.1023/A:1009260511939

Eyley, S., Thielemans, W., 2014. Surface modification of cellulose nanocrystals. Nanoscale 6, 7764–7779. https://doi.org/10.1039/C4NR01756K

Gibson, L.J., Ashby, M.F., 2014. Cellular Solids: Structure and Properties. Cambridge Solid State Science Series.

Gitli, T., Silverstein, M.S., 2008. Bicontinuous hydrogel–hydrophobic polymer systems through emulsion templated simultaneous polymerizations. Soft Matter 4, 2475. https://doi.org/10.1039/b809346f

Graeber, N., 2013. A Study of Fundamentals in Emulsion Templating for the Preparation of Macroporous Polymer Foams. Imperial College London Department of Chemical Engineering.

Gurevitch, I., Silverstein, M.S., 2010. Polymerized pickering HIPEs: Effects of synthesis parameters on porous structure. J. Polym. Sci. A Polym. Chem. 48, 1516–1525. https://doi.org/10.1002/pola.23911

Habibi, Y., 2014. Key advances in the chemical modification of nanocelluloses. Chem. Soc. Rev. 43, 1519–1542. https://doi.org/10.1039/C3CS60204D

Hainey, P., Huxham, I.M., Rowatt, B., Sherrington, D.C., Tetley, L., 1991. Synthesis and ultrastructural studies of styrene-divinylbenzene Polyhipe polymers. Macromolecules 24, 117–121. https://doi.org/10.1021/ma00001a019

Ikem, V.O., Menner, A., Bismarck, A., 2011. Tailoring the mechanical performance of highly permeable macroporous polymers synthesized via Pickering emulsion templating. Soft Matter 7, 6571. https://doi.org/10.1039/c1sm05272a

Ikem, V.O., Menner, A., Bismarck, A., 2010. High-Porosity Macroporous Polymers Sythesized from Titania-Particle-Stabilized Medium and High Internal Phase Emulsions. Langmuir 26, 8836–8841. https://doi.org/10.1021/la9046066

Ikem, V.O., Menner, A., Bismarck, A., 2008. High Internal Phase Emulsions Stabilized Solely by Functionalized Silica Particles. Angew. Chem. Int. Ed. 47, 8277–8279. https://doi.org/10.1002/anie.200802244

Kimmins, S.D., Cameron, N.R., 2011. Functional Porous Polymers by Emulsion Templating: Recent Advances. Adv. Funct. Mater. 21, 211–225. https://doi.org/10.1002/adfm.201001330

Klemm, D., Kramer, F., Moritz, S., Lindström, T., Ankerfors, M., Gray, D., Dorris, A., 2011. Nanocelluloses: A New Family of Nature-Based Materials. Angewandte Chemie International Edition 50, 5438–5466. https://doi.org/10.1002/anie.201001273

Lavoine, N., Bergström, L., 2017. Nanocellulose-based foams and aerogels: processing, properties, and applications. J. Mater. Chem. A 5, 16105–16117. https://doi.org/10.1039/C7TA02807E

Leal-Calderon, F., Schmitt, V., 2008. Solid-stabilized emulsions. Current Opinion in Colloid & Interface Science 13, 217–227. https://doi.org/10.1016/j.cocis.2007.09.005

Lépine, O., Birot, M., Deleuze, H., 2008. Influence of emulsification process on structure–properties relationship of highly concentrated reverse emulsion-derived materials. Colloid Polym Sci 286, 1273–1280. https://doi.org/10.1007/s00396-008-1891-1

Li, Y., Liu, X., Zhang, Z., Zhao, S., Tian, G., Zheng, J., Wang, D., Shi, S., Russell, T.P., 2018. Adaptive Structured Pickering Emulsions and Porous Materials Based on Cellulose Nanocrystal Surfactants. Angewandte Chemie International Edition 57, 13560–13564. https://doi.org/10.1002/anie.201808888

Liu, F., Zheng, J., Huang, C.-H., Tang, C.-H., Ou, S.-Y., 2018. Pickering high internal phase emulsions stabilized by protein-covered cellulose nanocrystals. Food Hydrocolloids 82, 96–105. https://doi.org/10.1016/j.foodhyd.2018.03.047

Liu, S., Jin, M., Chen, Y., Gao, H., Shi, X., Cheng, W., Ren, L., Wang, Y., 2017. High internal phase emulsions stabilised by supramolecular cellulose nanocrystals and their application as cell-adhesive macroporous hydrogel monoliths. Journal of Materials Chemistry B 5, 2671–2678. https://doi.org/10.1039/C7TB00145B

Meng, T., Gao, X., Zhang, J., Yuan, J., Zhang, Y., He, J., 2009. Graft copolymers prepared by atom transfer radical polymerization (ATRP) from cellulose. Polymer 50, 447–454. https://doi.org/10.1016/j.polymer.2008.11.011

Menner, A., Bismarck, A., 2006. New Evidence for the Mechanism of the Pore Formation in Polymerising High Internal Phase Emulsions or Why polyHIPEs Have an Interconnected Pore Network Structure. Macromol. Symp. 242, 19–24. https://doi.org/10.1002/masy.200651004

Menner, A., Ikem, V., Salgueiro, M., P. Shaffer, M.S., Bismarck, A., 2007a. High internal phase emulsion templates solely stabilised by functionalised titania nanoparticles. Chemical Communications 0, 4274–4276. https://doi.org/10.1039/B708935J

Menner, A., Verdejo, R., Shaffer, M., Bismarck, A., 2007b. Particle-Stabilized Surfactant-Free Medium Internal Phase Emulsions as Templates for Porous Nanocomposite Materials: poly-Pickering-Foams. Langmuir 23, 2398–2403. https://doi.org/10.1021/la062712u

Morandi, G., Heath, L., Thielemans, W., 2009. Cellulose Nanocrystals Grafted with Polystyrene Chains through Surface-Initiated Atom Transfer Radical Polymerization (SI-ATRP). Langmuir 25, 8280–8286. https://doi.org/10.1021/la900452a

572 Pang, B., Liu, H., Liu, P., Peng, X., Zhang, K., 2018. Water-in-oil Pickering emulsions stabilized by
573 stearoylated microcrystalline cellulose. Journal of Colloid and Interface Science 513, 629–637.
574 https://doi.org/10.1016/j.jcis.2017.11.079
575 Postek, M.T., Moon, R.J., Rudie, A.W., Bilodeu, M.A. (Eds.), 2013. , in: Production and Applications of
576 Cellulose Nanomaterials. TAPPI Press, Peachtree Corners, Ga.
577 Quell, A., de Bergolis, B., Drenckhan, W., Stubenrauch, C., 2016. How the Locus of Initiation Influences
578 the Morphology and the Pore Connectivity of a Monodisperse Polymer Foam. Macromolecules
579 49, 5059–5067. https://doi.org/10.1021/acs.macromol.6b00494
580 Schmitt, V., Destribats, M., Backov, R., 2014. Colloidal particles as liquid dispersion stabilizer: Pickering
581 emulsions and materials thereof. Comptes Rendus Physique 15, 761–774.
582 https://doi.org/10.1016/j.crhy.2014.09.010
583 Silverstein, M.S., 2014. Emulsion-templated porous polymers: A retrospective perspective. Polymer
584 55, 304–320. https://doi.org/10.1016/j.polymer.2013.08.068
585 Tai, H., Sergienko, A., Silverstein, M.S., 2001. High internal phase emulsion foams: Copolymers and
586 interpenetrating polymer networks. Polym. Eng. Sci. 41, 1540–1552.
587 https://doi.org/10.1002/pen.10853
588 Tang, J., Sisler, J., Grishkewich, N., Tam, K.C., 2017. Functionalization of cellulose nanocrystals for
589 advanced applications. Journal of Colloid and Interface Science 494, 397–409.
590 https://doi.org/10.1016/j.jcis.2017.01.077
591 Tasset, S., Cathala, B., Bizot, H., Capron, I., 2014. Versatile cellular foams derived from CNC-stabilized
592 Pickering emulsions. RSC Adv. 4, 893–898. https://doi.org/10.1039/C3RA45883K
593 Vílchez, A., Rodríguez-Abreu, C., Esquena, J., Menner, A., Bismarck, A., 2011. Macroporous Polymers
594 Obtained in Highly Concentrated Emulsions Stabilized Solely with Magnetic Nanoparticles.
595 Langmuir 27, 13342–13352. https://doi.org/10.1021/la2032576
596 Werner, A., Schmitt, V., Sèbe, G., Héroguez, V., 2019. Convenient Synthesis of Hybrid Polymer
597 Materials by AGET-ATRP Polymerization of Pickering Emulsions Stabilized by Cellulose
598 Nanocrystals Grafted with Reactive Moieties. Biomacromolecules 20, 490–501.
599 https://doi.org/10.1021/acs.biomac.8b01482
600 Werner, A., Sèbe, G., Héroguez, V., 2018. A new strategy to elaborate polymer composites *via* Pickering
601 emulsion polymerization of a wide range of monomers. Polym. Chem. 9, 5043–5050.
602 https://doi.org/10.1039/C8PY01022F
603 Wiley, R.M., 1954. Limited coalescence of oil droplets in coarse oil-in-water emulsions. Journal of
604 Colloid Science 9, 427–437. https://doi.org/10.1016/0095-8522(54)90030-6
605 Williams, J.M., Gray, A.J., Wilkerson, M.H., 1990. Emulsion stability and rigid foams from styrene or
606 divinylbenzene water-in-oil emulsions. Langmuir 6, 437–444.
607 https://doi.org/10.1021/la00092a026
608 Williams, J.M., Wrobleski, D.A., 1988. Spatial distribution of the phases in water-in-oil emulsions. Open
609 and closed microcellular foams from cross-linked polystyrene. Langmuir 4, 656–662.
610 https://doi.org/10.1021/la00081a027
611 Yang, Y., Cao, L., Li, J., Dong, Y., Wang, J., 2018. High-Performance Composite Monolith Synthesized via
612 HKUST-1 Stabilized HIPEs and Its Adsorptive Properties. Macromol. Mater. Eng. 303, 1800426.
613 https://doi.org/10.1002/mame.201800426
614 Yang, Y., Fang, Z., Chen, X., Zhang, W., Xie, Y., Chen, Y., Liu, Z., Yuan, W., 2017. An Overview of Pickering
615 Emulsions: Solid-Particle Materials, Classification, Morphology, and Applications. Front.
616 Pharmacol. 8. https://doi.org/10.3389/fphar.2017.00287
617 Zhang, H., Cooper, A.I., 2005. Synthesis and applications of emulsion-templated porous materials. Soft
618 Matter 1, 107. https://doi.org/10.1039/b502551f